Chapter 6

Electrical and Thermal Tuning of Band Structure and Defect Modes in Multilayer Photonic Crystals

Carlos G. Avendaño, Daniel Martínez and Ismael Molina

Additional information is available at the end of the chapter

http://dx.doi.org/10.5772/intechopen.70473

Abstract

We describe the main results previously studied concerning the thermal and electrical tuning of photonic band gap structures and the temperature-dependent defect modes in multilayer photonic liquid crystals using nematic liquid crystal slabs in a twisted configuration. In addition to this, we present new results regarding the electrical control of defect modes in such multilayer structures. In order to achieve this goal, we establish and solve numerically the equation governing the twisted nematic configurations under the action of the external electric field by assuming arbitrary anchoring conditions at the boundaries. After this, we write Maxwell's equations in a 4×4 matrix representation and, by using the matrix transfer technique, we obtain the transmittance and reflectance for incident circularly polarized waves.

Keywords: photonic band bap, electrical and thermal tuning, nematic liquid crystal, multilayer structure, defect mode

1. Introduction

Photonic crystals (PCs) are artificial structures with spatially periodic dielectric permittivity whose interesting optical properties have attracted the attention of the scientific community since the seminal works made by Yablonovitch [1] and John [2]. The most attractive attribute of these periodic structures is the existence of photonic band gaps (PBGs) in which the propagation of electromagnetic waves is prohibited for a specific wavelength range. In one-dimensional PCs, this phenomenon is usually called Bragg reflection. Liquid crystals (LCs) are anisotropic intermediate phases between the solid and liquid states of matter that possess positional and orientational order just like those of the solid crystals, and they can flow as a

conventional liquid [3]. For many decades, LCs have been used as optoelectronic substances on account of easy tunability of their properties under the stimuli of external agents as temperature, pressure and electromagnetic fields. This fact suggests the conception of new artificial structures by making a convenient combination of LCs with PCs, whose most prominent feature is the externally controlled PBG. First studies reported on this subject in three- and two-dimensional structures are attributed to Busch and John [4] and Leonard et al. [5], respectively. In [4], it was demonstrated the tunability of the PBG under the action of an external electric field meanwhile the temperature tuning when a nematic LC is infiltrated into the void regions of solid PCs is showed in [5].

Multilayer photonic liquid crystals (MPLCs) consisting of LCs alternated by transparent isotropic dielectric films have been previously studied. In Ref. [6], Ha et al. demonstrated experimentally simultaneous red, green and blue reflections (multiple PBGs) using the single-pitched polymeric cholesteric LC films. Later, Molina et al. [7] investigated the strong dependence of electric field on the PBG for incident waves of left- and right-circular polarization at arbitrary incidence angles using nematic liquid crystal (NLC) slabs in a twisted configuration. In a recent paper, Avendaño and Reyes [8] studied the optical band structure for reflectance and transmittance considering that the dielectric matrix of a similar one-dimensional photonic structure to that studied in Ref. [7] depends on temperature and wavelength. Twisted nematic LCs, where the molecular orientation exhibits a 90° twist, have proven technological advantages to control light flow. They have been used to switch effectively the pass of polarized light in nematic displays by means of a normally applied low-frequency electric field.

Surface anchoring plays an essential role in the science and technology of LCs. The structure of LCs in the bulk is different than that near the interface, and the boundary conditions established from this interface structure influence the behaviour of the LCs in the bulk. There are two cases of surface anchoring of particular interest. First, a strong anchoring case in which the molecules near the surface adopt a rigidly fixed orientation, and the anchoring energies are very large. Second, a weak anchoring case where the surface strengths are not strong enough to impose a well-defined molecular orientation at the interface, and the expression for the anchoring energy is some finite function that depends on the LC properties at the surface, the surface properties and the external fields (e.g., electric and magnetic fields) and temperature [9, 10]. Anchoring effects on the electrically controlled PBG in MPLCs were previously investigated by Avendaño [11]. They considered a generalization of the model studied in [7] for which arbitrary anchoring of the nematic at the boundaries is taken into account. They also found the nematic configuration versus the anchoring forces and the PBG under the action of a strong enough external field parallel to the periodicity axis, which is able to modify the configuration of the nematic-twisted LC in the whole material including at the boundaries of each nematic slab. Later, Avendaño and Martínez [12] theoretically exhibited that this system is able to produce an omnidirectional PBG that can be electrically controlled for circularly polarized incident waves. An omnidirectional PBG requires that there be no states in the given frequency range for propagation in any direction in the material for both polarizations, which implies the total reflectivity for all incident angles.

Resonant transmittance peaks in the PBG can be induced in PCs when defects are introduced in the periodic lattice. In this case, standing waves with a huge energy density are localized in

the proximity of the defects (defect modes). Ozaki et al. [13] developed the first tunable PC/LC hybrid structure by using a planar aligned NLC as a defect layer sandwiched between two one-dimensional periodical multilayers (dielectric materials with high- and low-refractive-index layers stacked alternatively) and demonstrated the electrical tuning of the defect modes. Thermal tunability of one-dimensional PC/LC cells was demonstrated by Arkhipkin et al. [14]. Electrical-dependent defect mode in PC/LC hybrid structures using a twisted nematic LC as defect layer was studied by Lin et al. [15] and Timofeev et al. [16]. Thermal tuning of defect modes in MPLCs using twisted nematic LC was recently shown in Ref. [8].

In this chapter, we describe the main results previously studied concerning the thermal and electrical tuning of PBG and the temperature-dependent defect modes in MPLCs using NLC slabs in a twisted configuration. In addition to this, we present new results regarding the electrical control of defect modes in MPLCs. In order to achieve this goal, we establish and solve numerically the equation governing the twisted nematic configurations under the action of the external electric field by assuming arbitrary anchoring conditions at the boundaries. After this, we write Maxwell's equations in a 4×4 matrix representation and, by using the matrix transfer technique, we obtain the transmittance and reflectance for incident circularly polarized waves.

2. Nematic-twisted configuration

As said above, we are focused on a 1D structure consisting in N NLC slabs in a twisted configuration alternated by N transparent isotropic dielectric films as it is illustrated in **Figure 1 (a)** and **(b)**. For each of the NLC cells, the nematic is sandwiched between two dielectric layers in such a way that its director is aligned parallel in both frontiers. A twist is then imposed on the NLC by rotating an angle $2\varphi_t$, one of the dielectric layers about its own normal direction. Because of the possibility of molecular reorientation under the influence of external stimuli, such as electromagnetic fields, the director $\boldsymbol{n}$ takes the general form

$$\boldsymbol{n} \equiv \boldsymbol{n}[\alpha(z), \varphi(z)] = [\cos\alpha(z)\cos\varphi(z),\ \cos\alpha(z)\sin\varphi(z),\ \sin\alpha(z)], \tag{1}$$

with $\alpha(z)$ and $\varphi(z)$, the polar (zenithal) and azimuthal angles made by $\boldsymbol{n}$ with the xy plane and the x-axis, respectively. For the present physical system and assuming small distortions in the nematic [17], the expression that describes the elastic energy density of the nematic is

$$f_{el} = \frac{1}{2}K_1(\nabla \cdot \boldsymbol{n})^2 + \frac{1}{2}K_2(\boldsymbol{n} \cdot \nabla \times \boldsymbol{n})^2 + \frac{1}{2}K_3(\boldsymbol{n} \times \nabla \times \boldsymbol{n})^2, \tag{2}$$

where the positive elastic moduli K_1, K_2 and K_3 refer to splay, twist and bend bulk deformations, respectively. At this point, it is important to mention that it has experimentally found that when the nematic temperature is increasing to its transition temperature T_{NI} (where the NLC becomes isotropic), a reduction of the values of the elastic moduli is induced [3, 17]. On the other hand, if we take into account the presence of an external electric field $\boldsymbol{E}$, the interaction of this field with the LC is described through the energy density $f_{em} = -\frac{1}{2}\mathrm{Re}\{\boldsymbol{E} \cdot \boldsymbol{D}^*\}$,

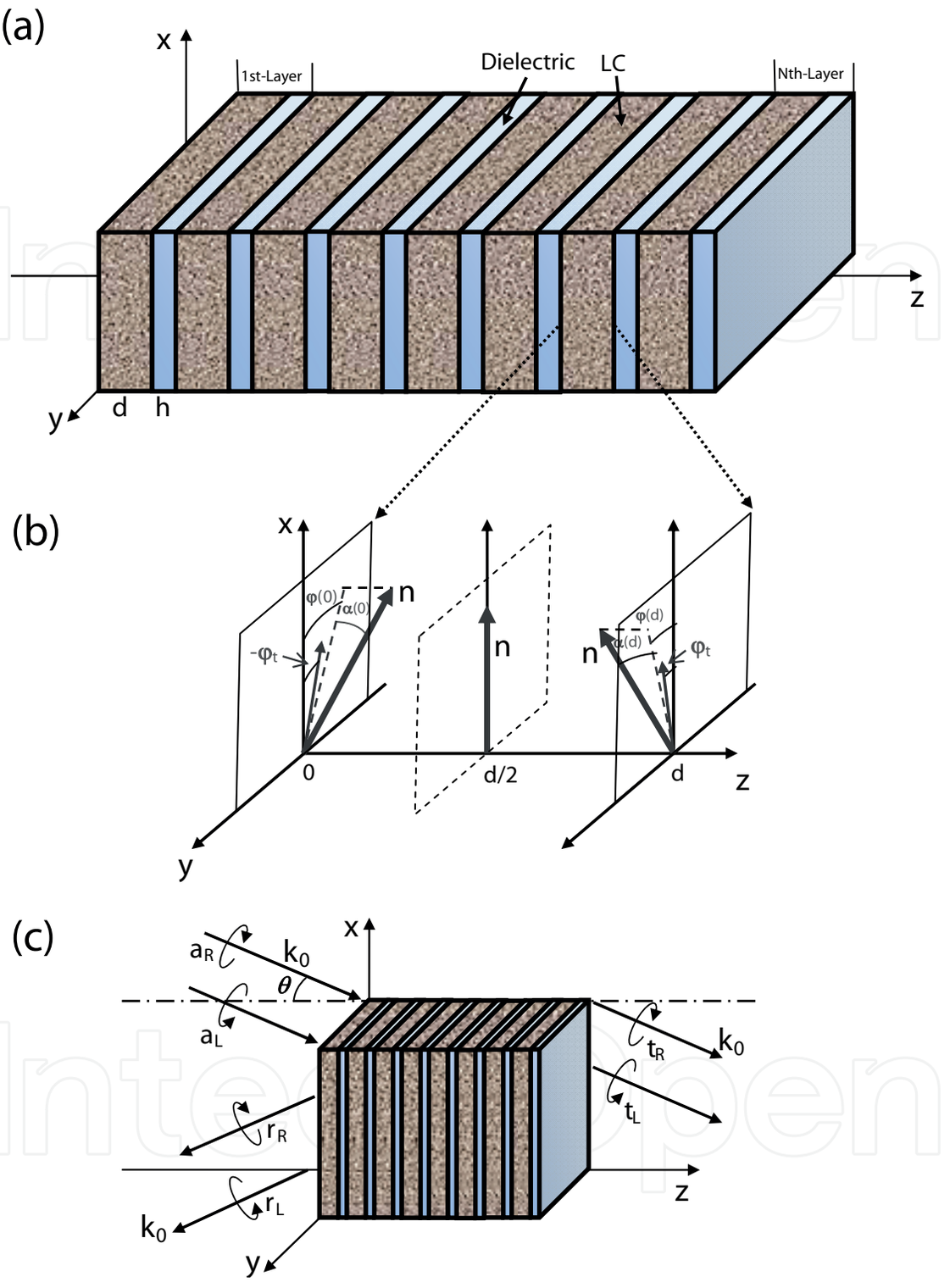

Figure 1. (a) Schematic of a MPLC consisting of N nematic LC slabs in a twisted configuration alternated by N transparent homogeneous isotropic dielectric films with thicknesses d and h, respectively. (b) Schematic of the polar α and azimuthal φ angles made by the director $\boldsymbol{n}$ with the xy-plane and the x-axis, respectively, at the boundaries of each of nematic LC slabs; the twist angle is given by ϕ_t and, at the middle of the slab, α=φ=0. (c) An obliquely incident electromagnetic field with wave vector $\mathbf{k}_0$ impinges on the structure in the xz-plane and it makes an angle θ with respect to the z-axis. Here, a_L and a_R represent the amplitudes of left- and right-circularly polarized components of incident wave, respectively, and r_L, r_R, t_L and t_R correspond to those of the reflected and transmitted waves.

http://dx.doi.org/10.5772/intechopen.70473

where we have assumed that the nematic follows the constitutive relation $\boldsymbol{D}=\varepsilon_0\boldsymbol{\varepsilon}\cdot\boldsymbol{E}$ characterized by the uniaxial dielectric tensor

$$\boldsymbol{\varepsilon} = \varepsilon_\perp \delta_{ij} + \varepsilon_a \boldsymbol{nn}, \tag{3}$$

with $\varepsilon_a=\varepsilon_\parallel-\varepsilon_\perp$ the dielectric anisotropy of the medium and ε_0 the permittivity of free space. Here, δ_{ij} is the Kronecker delta, $\varepsilon_\perp$ and $\varepsilon_\parallel$ denote the relative dielectric permittivity perpendicular and parallel to the nematic axis, respectively, and they are related to the ordinary n_o and extraordinary n_e refractive indices by $\varepsilon_\perp = n_o^2$ and $\varepsilon_\parallel = n_e^2$.

The study of confined nematic liquid crystals is strongly influenced by the physical properties of the boundary walls [18]. From the macroscopic-geometrical and microscopic interactions between the molecules of such surfaces and of the nematic, the alignment of the director $\boldsymbol{n}$ on the boundary surfaces, known as *anchoring*, can be completely determined. Once the anchoring conditions are established, the orientation of the NLC molecules at the substrate surface determined the director in the bulk.

Several methods and techniques for surface alignment have been developed [19, 20]. In the case of rubbed polymer films [21, 22], it has been observed that NLC molecules are *strongly anchored* at the surface, and the alignment is parallel to the grooves produced by the rubbing process. Also, the orientation of NLC molecules at the surfaces is preserved even if an external field (electric or magnetic) is applied and removed.

On the other hand, photoalignment [23] and nanostructuring polymer surfaces [24] are contact-free methods where it is induced a surface ordering that causes an anchoring of controllable strength, which corresponds to a *weak anchoring*. For this anchoring condition, alignment of the NLC molecules before and after the application of external fields is different.

Anchoring energy can be expressed in terms of the surface anchoring coefficients which are related to the interaction strength between the NLC and the wall substrate for the deviation of the easy axis along the correspondent directions. It is experimentally found that these coefficients are temperature dependent [18] and their values for specific NLCs can be obtained by using the dynamic light scattering [25]. Thus, if we write the director in terms of $\alpha(z)$ and $\varphi(z)$, as in expression (1), the anchoring energy of each NLC slab can be expressed in terms of the surface anchoring coefficients W_α and W_φ [26] as follows:

$$\begin{aligned} g^L &= W_\alpha \sin^2\alpha_m^L + W_\varphi \cos^2\alpha_m^L \sin^2\left(\varphi_m^L + \varphi_t\right) \\ g^R &= W_\alpha \sin^2\alpha_m^R + W_\varphi \cos^2\alpha_m^R \sin^2\left(\varphi_m^R - \varphi_t\right), \end{aligned} \tag{4}$$

which is an extension of the Rapini-Papoular model [9] and where $\alpha_m^L\left(\alpha_m^R\right)$ and $\varphi_m^L\left(\varphi_m^R\right)$ are the polar and azimuthal angles at the left (right) boundary of each NLC, respectively, and φ_t the twist angle. These anchoring coefficients are measured in energy per area units.

Thus, strong anchoring conditions are achieved when the anchoring coefficients are sufficiently large and can be modelled by considering that $W_\alpha\to\infty$ and $W_\varphi\to\infty$. In contrast, for weak anchoring conditions, it is taken that $W_\alpha\to 0$ and $W_\varphi\to 0$. Another criterion to establish whether the anchoring is strong or weak is based on the *extrapolation length* [27].

Thus, the equations governing the equilibrium configuration of the system are obtained by considering specific anchoring conditions and by minimizing the total free energy

$$F = \int_V (f_{el} + f_{em}) dV + \frac{1}{2}\int_{S_0} g^L dS + \frac{1}{2}\int_{S_d} g^R dS, \tag{5}$$

that can be achieved by considering strong or weak anchoring conditions.

2.1. Strong anchoring

Let us assume that the structure shown in **Figure 1(a)** is subjected to a DC electric field $\boldsymbol{E}_{dc}$=(0, 0,E_{dc}) parallel to z-axis, and we consider that the orientation of the director at the surfaces of each nematic cell are fixed and given by α=0°, $\varphi\left[z_m^L = (m-1)(d+h)\right] = -\varphi_t$ and $\varphi\left[z_m^R = (m-1)(d+h)+d\right] = \varphi_t$ for m=1,2,3, … ,N. Here, z_m^L and z_m^R represent the positions of the left and right boundaries of the N nematic layers, respectively. Under these circumstances and by using a standard variational calculus procedure, the minimum free-energy condition δF=0 together with the restriction $\delta \boldsymbol{n}$=0 at the surface of each slab generate the equations [12]

$$0 = f(\alpha)\frac{d^2\alpha}{dz^2} + \frac{1}{2}\frac{df(\alpha)}{d\alpha}\left(\frac{d\alpha}{dz}\right)^2 - \frac{1}{2}\frac{dg(\alpha)}{d\alpha}\left(\frac{d\varphi}{dz}\right)^2 + \frac{1}{2}\left(\frac{\sigma}{d}\right)^2 \sin 2\alpha, \tag{6}$$

$$0 = g(\alpha)\frac{d^2\varphi}{dz^2} + \frac{dg(\alpha)}{d\alpha}\frac{d\alpha}{dz}\frac{d\varphi}{dz}, \tag{7}$$

where we have defined the dimensionless parameter $\sigma^2 = \varepsilon_0 \varepsilon_a E_{dc}^2 / \left(K_1/d^2\right)$ which represents the ratio between the electric and elastic energies. The functions $f(\alpha)$ and $g(\alpha)$ are defined as

$$\begin{aligned} f(\alpha) &= \cos^2\alpha + \frac{K_3}{K_1}\sin^2\alpha \\ g(\alpha) &= \left(\frac{K_2}{K_1}\cos^2\alpha + \frac{K_3}{K_1}\sin^2\alpha\right)\cos^2\alpha. \end{aligned} \tag{8}$$

In absence of the dc electric field, the polar angle $\alpha(z)$=0° for any value of z and, the solution of Eqs. (6) and (7) is simply

$$\varphi_m(z) = \frac{2\varphi_t}{d}(z - (m-1)(d+h)) - \varphi_t, \tag{9}$$

where $\varphi_m(z)$ represents the configuration of the mth layer in the region $(m-1)(d+h) \le z \le (m-1)(d+h)+d$ and the nematic director (1) is reduced to

$$\boldsymbol{n} \equiv \boldsymbol{n}[\varphi(z)] = [\cos\varphi(z),\ \sin\varphi(z), 0]. \tag{10}$$

2.2. Weak anchoring

In this case, we consider a free-end-point variation for which the director orientation is affected by the existence of finite anchoring coefficients [12]. This minimization procedure leads to the

same set of coupled equations given by (6) and (7) subjected to boundary conditions at each layer:

$$\left.\frac{d\alpha}{dz}\right|_{z=z_m^L} = \left.\frac{1}{d\,\Gamma_\alpha}\frac{\left(1-\Gamma\sin^2\left(\varphi+\varphi_t\right)\right)\sin 2\alpha}{f(\alpha)}\right|_{z=z_m^L}, \tag{11}$$

$$\left.\frac{d\alpha}{dz}\right|_{z=z_m^R} = -\left.\frac{1}{d\,\Gamma_\alpha}\frac{\left(1-\Gamma\sin^2\left(\varphi-\varphi_t\right)\right)\sin 2\alpha}{f(\alpha)}\right|_{z=z_m^R}, \tag{12}$$

$$\left.\frac{d\varphi}{dz}\right|_{z=z_m^L} = \left.\frac{\Gamma}{d\,\Gamma_\alpha}\frac{\sin 2\left(\varphi+\varphi_t\right)\cos^2\alpha}{g(\alpha)}\right|_{z=z_m^L}, \tag{13}$$

$$\left.\frac{d\varphi}{dz}\right|_{z=z_m^R} = -\left.\frac{\Gamma}{d\,\Gamma_\alpha}\frac{\sin 2\left(\varphi-\varphi_t\right)\cos^2\alpha}{g(\alpha)}\right|_{z=z_m^R}, \tag{14}$$

With $\Gamma_\alpha=1/\gamma_a$,$\Gamma=\gamma_\varphi/\gamma_a$, $\gamma_a=W_\alpha d/K_1$ and $\gamma_\varphi=W_\varphi d/K_1$.

3. Electromagnetic propagation in a layered medium

The interaction between electromagnetic fields and matter is governed by Maxwell's equations and their corresponding constitutive equations. Optical propagation in layered media can be studied by conveniently writing Maxwell's equations in a 4×4 matrix representation. In this matrix representation, the boundary conditions of waves impinging on material can be imposed in such a way that the transfer and scattering matrix formalism to obtain the transmittances and reflectances can be used in a natural way [28, 29].

3.1. 4 × 4 matrix representation

In systems where boundary conditions cannot be avoided, Maxwell's equations require the continuity of tangential components of electric **E** and magnetic **H** fields at the boundaries. In studying the optical properties of dielectric layers which are confined between parallel walls, it is useful to write the set of Maxwell's equations in a representation where only appears, at the same time, the transversal components of **E** and **H** (two components for **E** and two components for **H**). This formalism is frequently referred to as Marcuvitz-Schwinger representation [30]. If we consider that the optical properties of a multilayer structure depends only on spatial variable z, we define the time-harmonic transversal four-vector

$$\mathbf{\Psi}(x,y,z) = \boldsymbol{\psi}(z)e^{ik_x x-i\omega t} = \begin{pmatrix} e_x(z) \\ e_y(z) \\ h_x(z) \\ h_y(z) \end{pmatrix} e^{ik_x x}e^{-i\omega t}, \tag{15}$$

with ω the angular frequency of the propagating wave and k_x the transversal component of the wave vector. Maxwell's equations, inside a nonmagnetic medium, can be written in the following matrix form:

$$\frac{\partial \boldsymbol{\psi}(z)}{\partial z} = i\boldsymbol{A}(z).\boldsymbol{\psi}(z), \tag{16}$$

for which the 4×4 matrix $\boldsymbol{A}(z)$ is given by

$$\mathbf{A}(z) = \begin{pmatrix} -\frac{k_x\varepsilon_{zx}}{k_0\varepsilon_{zz}} & -\frac{k_x\varepsilon_{zy}}{k_0\varepsilon_{zz}} & 0 & 1-\frac{k_x^2}{k_0^2\varepsilon_{zz}} \\ 0 & 0 & -1 & 0 \\ -\varepsilon_{yx}+\frac{\varepsilon_{yz}\varepsilon_{zx}}{\varepsilon_{zz}} & \frac{k_x^2}{k_0^2}-\varepsilon_{yy}+\frac{\varepsilon_{yz}\varepsilon_{zy}}{\varepsilon_{zz}} & 0 & \frac{k_x\varepsilon_{yz}}{k_0\varepsilon_{zz}} \\ \varepsilon_{xx}-\frac{\varepsilon_{xz}\varepsilon_{zx}}{\varepsilon_{zz}} & \varepsilon_{xy}-\frac{\varepsilon_{xz}\varepsilon_{zy}}{\varepsilon_{zz}} & 0 & -\frac{k_x\varepsilon_{xz}}{k_0\varepsilon_{zz}} \end{pmatrix} \tag{17}$$

where ε_{ij} (i,j=x,y,z) represents the elements of dielectric matrix in the structure, k_0=$2\pi/\lambda$=ω/c is the wavenumber in free space, λ is the wavelength and c denotes the speed of light in vacuum. Also the fields $\mathbf{e}(z)$=($e_x(z)$, $e_y(z)$, $e_z(z)$) and $\mathbf{h}(z)$=($h_x(z)$, $h_y(z)$, $h_z(z)$) are related to the electric $\mathbf{E}(z)$ and magnetic $\mathbf{H}(z)$ fields by the following expressions $\mathbf{e}(z) \equiv Z_0^{-1/2}\mathbf{E}(z)$ and $\mathbf{h}(z) \equiv Z_0^{1/2}\mathbf{H}(z)$, with $Z_0 = \sqrt{\mu_0/\epsilon_0}$ the impedance in vacuum, ε_0 and μ_0 the permittivity and permeability of free space, respectively.

For a homogeneous and isotropic dielectric medium, the matrix $\boldsymbol{\varepsilon}(z)$ is diagonal and independent of the position, whereas for a nematic slab, $\boldsymbol{\varepsilon}(z)$ depends on the local orientation of the principal axis of the liquid crystal molecules characterized by expression (3).

3.2. Boundary condition

Let us consider a multilayer structure where each of the layers is confined between two planes, and the whole structure is surrounded by air. An electromagnetic wave impinging from the left side of the multilayer structure will propagate through the sample, and it will be transmitted and reflected outside the medium (see **Figure 1 (c)**).

The general solution of the differential equation (16) for electromagnetic waves propagating in homogeneous media is the superposition of four plane waves: two left-going and two right-going waves. With this in mind, we state the procedure to find the amplitudes of the transmitted and reflected waves in terms of incident ones (at plane z=0). This implies the definition of the following quantities [31]:

(i) The propagation matrix $\boldsymbol{U}(0,z)$ that is implicitly defined by the equations

$$\boldsymbol{\psi}(z) = \boldsymbol{U}(0,z).\boldsymbol{\psi}(0), \qquad \boldsymbol{U}(0,0) = \mathbf{1}, \tag{18}$$

where $\mathbf{1}$ is the identity matrix and $\boldsymbol{U}(0,z)$ satisfies the same propagation equation (16) found for $\boldsymbol{\psi}$:

$$\partial_z \boldsymbol{U}(0,z) = i\boldsymbol{A}(z).\boldsymbol{U}(0,z). \tag{19}$$

This propagation matrix gives the right-side field amplitudes of the multilayer structure as function of the left-side ones.

(ii) For a specific value $z=z_0$, the transfer matrix is defined as $\boldsymbol{U}(0,z_0)$.

(iii) The scattering matrix $\boldsymbol{S}$ giving the output field as function of the incident one. The matrix $\boldsymbol{S}$ is defined through the relation $\boldsymbol{\alpha}_{out}=\boldsymbol{S}\cdot\boldsymbol{\alpha}_{in}$, where $\boldsymbol{\alpha}_{in}$ and $\boldsymbol{\alpha}_{out}$ are the amplitudes of the in-going and out-going waves.

To find out $\boldsymbol{S}$, the field must expressed, in any one of the external media, as a superposition of planes waves by setting:

$$\boldsymbol{\psi}=\boldsymbol{T}\cdot\boldsymbol{\alpha};\qquad \boldsymbol{U}_{\boldsymbol{\alpha}}(0,z_0)=\boldsymbol{T}^{-1}\cdot\boldsymbol{U}(0,z_0)\cdot\boldsymbol{T}, \tag{20}$$

where $\boldsymbol{\alpha}=\left(a_1^+,a_2^+,a_1^-,a_2^-\right)^T$.

The relation $\boldsymbol{\psi}=\boldsymbol{T}\cdot\boldsymbol{\alpha}$ can be interpreted as a basis change in the four dimensional space of the *state vectors* $\boldsymbol{\psi}$. The columns of $\boldsymbol{T}$ are the $\boldsymbol{\psi}$ vectors representing the four plane waves generated by the incident waves in the two external media (assumed as identical). The elements of vector $\boldsymbol{\alpha}$ are the amplitudes of the four plane wave. The choice of the new basis could be different depending on the particular problem. By setting

$$\boldsymbol{U}(\boldsymbol{\alpha})=\begin{pmatrix}\boldsymbol{U}_{ff} & \boldsymbol{U}_{bf}\\ \boldsymbol{U}_{fb} & \boldsymbol{U}_{bb}\end{pmatrix}, \tag{21}$$

the scattering matrix writes:

$$\boldsymbol{S}=\begin{pmatrix}\boldsymbol{U}_{ff}-\boldsymbol{U}_{bf}\boldsymbol{U}_{bb}^{-1}\boldsymbol{U}_{fb} & \boldsymbol{U}_{bf}\boldsymbol{U}_{bb}^{-1}\\ -\boldsymbol{U}_{bb}^{-1}\boldsymbol{U}_{fb} & \boldsymbol{U}_{bb}^{-1}\end{pmatrix}. \tag{22}$$

where the symbols + and f (− and b) mean forward (backward) propagating waves.

We point out that the methods of transfer and scattering matrices are very useful in studying the plane wave transmission and reflection from surfaces of multilayer structures.

Differential equation (16) can be formally integrated over a certain distance z_0 of the medium

$$\boldsymbol{\psi}(z_0)=e^{i\int_0^{z_0}\boldsymbol{A}(z')dz'}\cdot\boldsymbol{\psi}(0), \tag{23}$$

and by straight comparison of Eqs. (18) and (23), the transfer matrix $\boldsymbol{U}(0,z_0)$ is defined as:

$$\boldsymbol{U}(0,z_0)=e^{i\int_0^{z_0}\boldsymbol{A}(z')dz'}, \tag{24}$$

where plane waves are incident and reflected in the half-space $z<0$, and plane waves are transmitted on the half-space $z>z_0$.

It can be seen immediately that the problem of finding $\boldsymbol{U}(0,z_0)$ is reduced to find a method to integrate expression (24) on the whole multilayer structure. Because of the non-homogeneity of the medium proposed here, we consider it as broken up into many very thin parallel layers, each of them with homogeneous anisotropic optical parameters [32]. In this way, $\boldsymbol{U}(0,z_0)$ is obtained by multiplying iteratively the matrix for each sublayer from $z = 0$ to $z = z_0$.

3.3. Transmission and reflection by multilayer structures

As said above, the general solution of the differential equation (16) for electromagnetic waves propagating in homogeneous media is the superposition of forward and backward propagating waves. The obliquely incident and reflected electromagnetic fields in free half-space $z \leq 0$ (**Figure 1 (c)**), for an arbitrary polarization state which are solutions of equation (16), can be expressed as:

$$\begin{pmatrix} \mathbf{e} \\ \mathbf{h} \end{pmatrix}_{inc} = \begin{pmatrix} [a_L(i\mathbf{u} - \mathbf{v}_+) - a_R(i\mathbf{u} + \mathbf{v}_+)] \exp(ik_{0z}z) \\ -i[a_L(i\mathbf{u} - \mathbf{v}_+) + a_R(i\mathbf{u} + \mathbf{v}_+)] \exp(ik_{0z}z) \end{pmatrix} \tag{25}$$

and

$$\begin{pmatrix} \mathbf{e} \\ \mathbf{h} \end{pmatrix}_{ref} = \begin{pmatrix} -[r_L(i\mathbf{u} - \mathbf{v}_-) - r_R(i\mathbf{u} + \mathbf{v}_-)] \exp(-ik_{0z}z) \\ i[r_L(i\mathbf{u} - \mathbf{v}_-) + r_R(i\mathbf{u} + \mathbf{v}_-)] \exp(-ik_{0z}z) \end{pmatrix}, \tag{26}$$

where $\mathbf{k}_0=(k_{0x}, k_{0y}, k_{0z})=k_0(\sin\theta, 0, \cos\theta)$ is the wave vector of the incident wave making an angle θ with respect to the z-axis, a_L and a_R represent the amplitudes of left- and right-circularly polarized (LCP and RCP) components of incident wave, respectively, and r_L and r_R correspond to those of the reflected wave (see **Figure 1(c)**). The unit vectors $\mathbf{u}$ and $\mathbf{v}$ are defined as

$$\mathbf{u} = \frac{\mathbf{u}_y}{\sqrt{2}}, \qquad \mathbf{v}_\pm = \frac{\mp \cos\theta \mathbf{u}_x + \sin\theta \mathbf{u}_z}{\sqrt{2}}, \tag{27}$$

with $\mathbf{u_x}, \mathbf{u_y}, \mathbf{u_z}$ the triad of Cartesian unit vectors. In the region $z \geq z_0$, the transmitted electromagnetic field is

$$\begin{pmatrix} \mathbf{e} \\ \mathbf{h} \end{pmatrix}_{tr} = \begin{pmatrix} [t_L(i\mathbf{u} - \mathbf{v}_+) - t_R(i\mathbf{u} + \mathbf{v}_+)] \exp(ik_{0z}(z - N(d+h) - h)) \\ -i[t_L(i\mathbf{u} - \mathbf{v}_+) + t_R(i\mathbf{u} + \mathbf{v}_+)] \exp(ik_{0z}(z - N(d+h) - h)) \end{pmatrix}, \tag{28}$$

where t_L and t_R are the amplitudes of LCP and RCP components, respectively, of transmitted wave. As the tangential components of $\mathbf{e}$ and $\mathbf{h}$ must be continuous across the planes z=0 and z=z_0, the boundary values $\boldsymbol{\psi}(0)$ and $\boldsymbol{\psi}(z_0)$ can be fixed as:

$$\boldsymbol{\psi}(0) = \frac{\boldsymbol{P}}{\sqrt{2}} \cdot \begin{pmatrix} a_R \\ a_L \\ r_R \\ r_L \end{pmatrix} \quad \text{and} \quad \boldsymbol{\psi}(z_0) = \frac{\boldsymbol{P}}{\sqrt{2}} \cdot \begin{pmatrix} t_R \\ t_L \\ 0 \\ 0 \end{pmatrix}, \tag{29}$$

with

$$\mathbf{P} = \begin{pmatrix} \cos\theta & \cos\theta & \cos\theta & \cos\theta \\ -i & i & i & -i \\ i\cos\theta & -i\cos\theta & i\cos\theta & -i\cos\theta \\ 1 & 1 & -1 & -1 \end{pmatrix}. \tag{30}$$

By using Eqs. (23), (24) and (29), the problem of reflection-transmission can be established as follows

$$\begin{pmatrix} t_R \\ t_L \\ 0 \\ 0 \end{pmatrix} = \boldsymbol{M} \cdot \begin{pmatrix} a_R \\ a_L \\ r_R \\ r_L \end{pmatrix}, \tag{31}$$

where $\boldsymbol{M}=\boldsymbol{P}^{-1}\cdot\boldsymbol{U}(0,z_0)\cdot\boldsymbol{P}$ and $\boldsymbol{U}(0,z_0)$ are defined in (24). Notice that the matrix equation (31) gives a set of coupled equations relating the amplitudes a_L, a_R, r_L and r_R (from $z \le 0$) to the transmitted amplitudes t_L and t_R (for $z \ge z_0$).

The scattering matrix $\boldsymbol{S}$ relates the amplitudes t_L, t_R, r_L and r_R to the known incident amplitudes a_L and a_R. This relation can be expressed in terms of matrix $\boldsymbol{M}$ as [33]

$$\begin{pmatrix} t_R \\ t_L \\ r_R \\ r_L \end{pmatrix} = \boldsymbol{S} \cdot \begin{pmatrix} a_R \\ a_L \end{pmatrix}. \tag{32}$$

where

$$\boldsymbol{S} = \begin{pmatrix} t_{RR} & t_{RL} \\ t_{LR} & t_{LL} \\ r_{RR} & r_{RL} \\ r_{LR} & r_{LL} \end{pmatrix} = (\boldsymbol{Q}_1 - \boldsymbol{M}\boldsymbol{Q}_2)^{-1}(\boldsymbol{M}\boldsymbol{Q}_1 - \boldsymbol{Q}_2) \tag{33}$$

and

$$\boldsymbol{Q}_1 = \begin{pmatrix} 1 & 0 & 0 & 0 \\ 0 & 1 & 0 & 0 \\ 0 & 0 & 0 & 0 \\ 0 & 0 & 0 & 0 \end{pmatrix}, \quad \boldsymbol{Q}_2 = \begin{pmatrix} 0 & 0 & 0 & 0 \\ 0 & 0 & 0 & 0 \\ 0 & 0 & 1 & 0 \\ 0 & 0 & 0 & 1 \end{pmatrix}. \tag{34}$$

Co-polarized coefficients have both subscripts identical meanwhile cross-polarized coefficients have different subscripts. The square of the amplitudes of t and r is the corresponding transmittance and reflectance, respectively; thus, $T_{RR}=|t_{RR}|^2$ is the co-polarized transmittance corresponding to the transmission coefficient t_{RR}, $T_{RL}=|t_{RL}|^2$ is the cross-polarized transmittance

corresponding to the transmission coefficient t_{RL}, and so forth. In the absence of dissipation of energy inside the sample, the principle of conservation of energy must be satisfied from which we have that

$$T_{RR} + T_{LR} + R_{RR} + R_{LR} = 1 \qquad \text{and} \qquad T_{RL} + T_{LL} + R_{RL} + R_{LL} = 1. \tag{35}$$

Before ending this section, we mention that an alternative way to find the transmission and reflection coefficients is using the expressions given by (21) and (22). Also, the system of equations (31) can be solved numerically to find the scattering matrix.

4. Numerical results and discussion

In previous sections, we have presented in detail a general mathematical formalism to determine the reflectances and transmittances by multilayer structures. In this section, we apply this formalism to MPLCs using NLC slabs in a twisted configuration considering that circularly polarized light impinges on the structure in order to analyse the optical spectra and their dependence on external agents. In particular, we describe the main results previously studied concerning the thermal and electrical tuning of optical spectra and the temperature-dependent defect modes. In addition to this, we present new results regarding the electrical control of defect modes.

4.1. Electrical tuning of band structure and defect mode

In this section, we present the influence of the electric field on the optical band structure and defect mode by considering arbitrary anchoring conditions at the boundaries. To this aim, the equilibrium configuration of each NLC layer as a function of σ is obtained by solving the second order differential equations (6) and (7) for $\alpha(z)$ and $\varphi(z)$ subjected to the conditions expressed in Eqs. (11)–(14). Then, this configuration is substituted into Eq. (23) in order to obtain the transfer matrix $\boldsymbol{M}$ as function of σ for circularly polarized incident waves.

Numerical calculations were performed by considering a NLC phase 5CB for which K_1=0.62 × $10^{-11}N$, K_2=0.39 × $10^{-11}N$, K_3=0.82 × $10^{-11}N$ [17] and refractive indices at optical frequencies $n_o = \sqrt{\varepsilon_\perp} = 1.53$ and $n_e = \sqrt{\varepsilon_\parallel} = 1.717$. The twist angle is taken $2\varphi_t$=90°, and the homogeneous isotropic dielectric medium is zinc sulphide (ZnS) with refractive index n_d=2.35. The MPLC consists of N=11 NLC layers alternating with N=11 dielectric slabs with the same thickness. Finally, we report our results parameterizing all the spatial variables by the NLC thickness d. In this way, the dimensionless thickness of each NLC cell is $h'=d/d=1$, whereas for each ZnS slab is $h'=h/d=1$, and so forth.

Due to the competition between orientation produced by influence of the external electric field and by surface anchoring effects, we expect a deformation in the NLC only above a certain critical value σ_c. This critical electric field is expected to be maximum for the case of strong anchoring conditions, whereas for the weak anchoring case, σ_c will decrease as the surface forces get smaller [7, 11].

4.1.1. Strong anchoring conditions

For strong anchoring conditions, the orientation of the nematic molecules at the walls of each NLC is specified in Section 2.1. The curves for $\alpha(z)$ and $\varphi(z)$ are shown in **Figure 2(a)** and **(b)**, respectively, as function of dimensionless variable $w = z/d$ above the critical value $\sigma_c = 3.26$. As it can be noticed in **Figure 2(a)**, an increment in the electric field involves the augmentation in the polar angle α. Owing to the influence of the external field, the nematic molecules tend to be aligned parallel to it (z-axis). As expected, for $\sigma < \sigma_c$, $\alpha = 0°$ for all values of w, which means that the director in this case is perpendicular to the z-axis. In **Figure 2(b),** we observe that for $\sigma < \sigma_c$, the curves for azimuthal angle φ are reduced to straight lines with slope equal to $2\varphi_t = 90°$, that corresponds to the configuration of a pure twisted NLC. Above the critical value, the strong anchoring condition is really dominant on the parameter φ as the electric field increases. Indeed, most of molecules tend to spread far from xz plane.

Figure 3 exhibits the co-polarized and cross-polarized transmittances and reflectances for LCP and RCP waves impinging normally on the structure as function of the dimensionless parameter d/λ for continuous values of the electric field above the critical value σ_c (it is worth to mention that below this value, the not-shown curves are very similar to that of $\sigma = \sigma_c$). Note the strong influence of σ on the transmission and reflection spectra in enhancing and extinguishing bands. Indeed, **Figure 3** clearly shows that for $\sigma = \sigma_c$, the curves for transmittances exhibit several stop bands of different widths in the plotted interval and, as σ increases, each stop band gets wider for co-polarized transmittances T_{RR} and T_{LL}. Also, cross-polarized transmittances T_{LR} and T_{RL} are totally absent for high enough values of the electric field. On the other hand, at the critical value, co-polarized reflectances R_{RR} and R_{LL} exhibit narrow-reflection bands with relatively high amplitudes and cross-polarized reflectances R_{LR} and R_{RL} show one-dominant high-reflection band. In this case, co-polarized reflectances reduce their band amplitudes practically to zero, and reflection bands of cross-polarized reflectances are highly enhanced for larger values of σ. These optical properties allow us to use this MPLC as an electrically shiftable universal rejection filter for incident RCP and LCP waves where, by

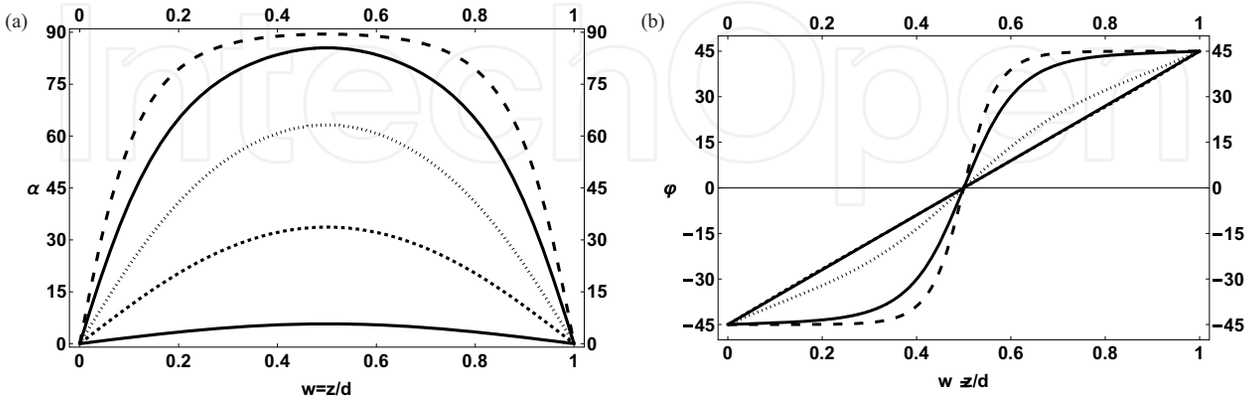

Figure 2. (a) Curves of the polar angle α as function of dimensionless variable w at different values of σ: $\sigma=\sigma_c+0.005$ (solid line), $\sigma=3.5$ (dashed line), $\sigma=4.5$ (dotted line), $\sigma=8$ (dot-dashed line) and $\sigma=13.5$ (large dashed line). Below the critical value σ_c, $\alpha=0^{\circ}$. (b) Curves of the azimuthal angle φ at the same values of σ as in (a). Below the critical value σ_c, the curve is a straight line with slope $2\varphi_t=90^{\circ}$.

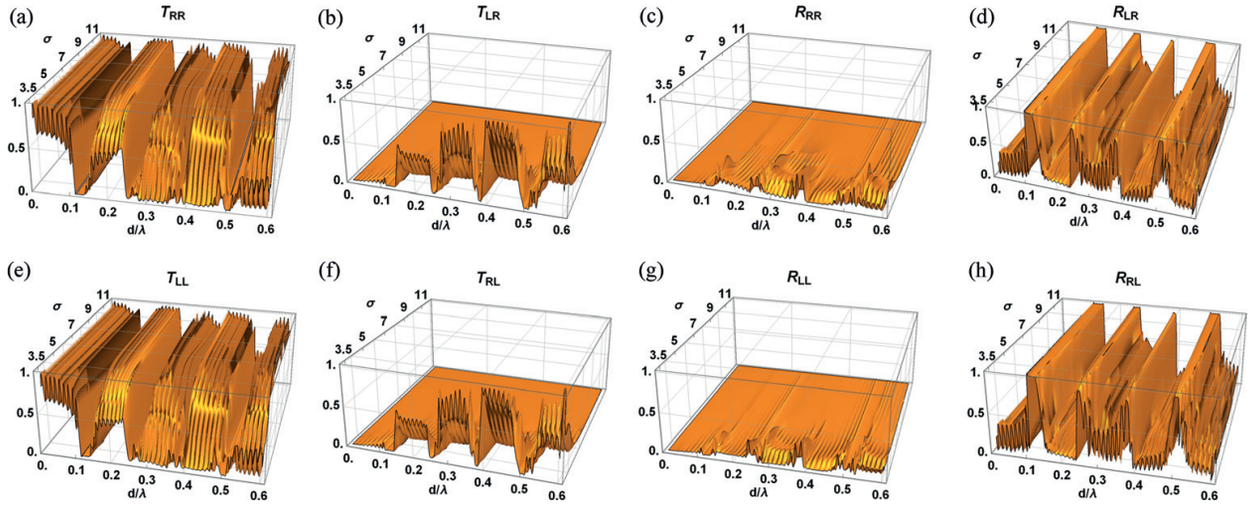

Figure 3. (a)–(h) Plots of co-polarized and cross-polarized reflectances and transmittances for LCP and RCP waves impinging normally on a MPLC as function of the dimensionless parameter d/λ and continuous values of σ within the interval $\sigma_c < \sigma < 13$.

increasing the electric field, one can highly enhance the cross-polarized reflection bands and supress the co-polarized ones.

In [7], it is shown that for a fixed value of σ the band structure of the reflectances and transmittances are shifted towards smaller wavelength regions as the incident angle θ increases. This behaviour results from the fact that for plane electromagnetic waves propagating obliquely with respect to the layer interfaces, only the normal component of the wave vector is involved in the photonic band formation. Hence, as the incident angle augments, the relative position of the bands is moved towards smaller wavelengths.

If one of the layers possesses a different size compared with the remaining ones, this layer can act as a defect, and an optical defect mode can be induced. Here, we specifically consider that the middle NLC-ZnS stack of the MPLC has a different size compared with the remaining ones. We choose specific values $d_d=2d^{'}$ and $h_d=2h^{'}$, where d_d and h_d are the dimensionless thicknesses of the NLC and ZnS defect layers, respectively. **Figure 4(a)** and **(b)** displays the defect mode induced in the photonic band of the co-polarized transmittance T_{RR} and cross-polarized reflectance R_{LR}, respectively, by LCP waves impinging normally on the MPLC. We notice that as the parameter σ increases two important facts occur: (i) two defect modes with small amplitude are induced within the first stop band (see **Figure 3**) which gradually merge into only one; the position of the defect mode possessing the largest wavelength moves toward regions of smaller wavelengths, keeping fixed the position of the other one and (ii) the amplitude of the defect modes gets larger. Physically, the origin of the defect mode is the phase change due to the variation in the optical path length caused by the defective medium. Once the defect mode is created at specific position, it can be controlled by inducing reorientation in the nematic molecules by means of an external electric field [7]. Indeed, since the refractive index of the LC depends on the angle β between the wave vector **k** of the electromagnetic wave in the LC and the local orientation of the director ***n***, the refractive index (and the optical path length) can be changed by varying β. At normal incidence and $\sigma < \sigma_c$, $\beta = 90^{\circ}$ for all positions z.

http://dx.doi.org/10.5772/intechopen.70473

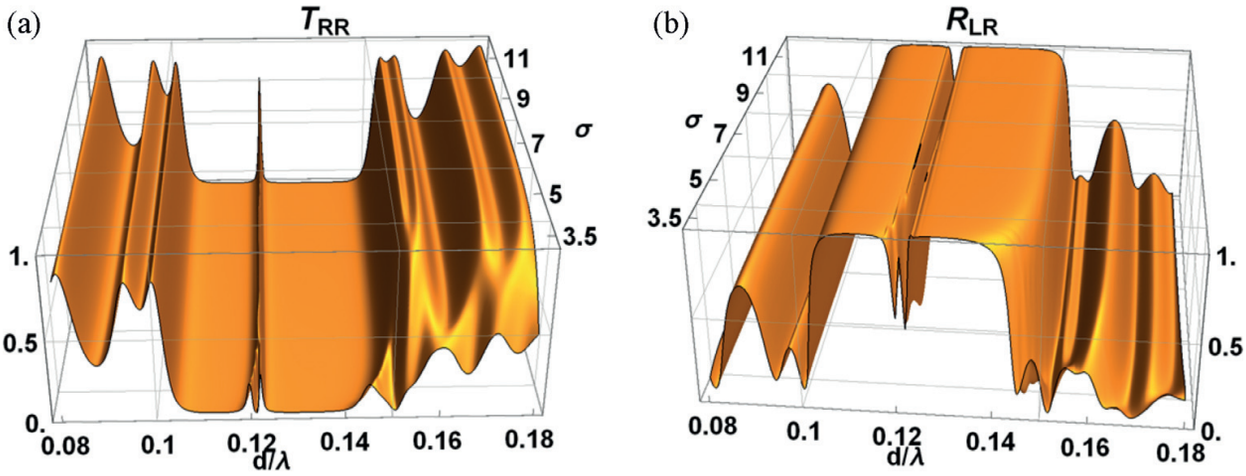

Figure 4. (a) At normal incidence, plots of co-polarized transmittance T_{RR} for LCP incident waves as function of the dimensionless parameter d/λ and continuous values of σ. (b) At normal incidence, cross-polarized reflectance R_{LR} for LCP incident waves at the same values of σ as in (a).

Nevertheless, as σ increases, most of the molecules tend to be aligned parallel to z-axis (see **Figure 2(a)**) and $\beta \rightarrow 0^\circ$. These results show that the amplitude of defect mode and its position can be tuned by a DC electric field.

4.1.2. Weak anchoring conditions

It is experimentally found that for a LC phase 5CB, the polar anchoring γ_α is of the order of 10^1, and this value is one or two orders stronger than the azimuthal anchoring γ_φ [34]. Under these considerations, the values of the dimensionless anchoring parameters are taken as $\Gamma=\Gamma_\alpha=0.1$.

The curves for $\alpha(z)$ and $\varphi(z)$ are shown in **Figure 5(a)** and **(b)**, respectively, as function of dimensionless variable $w=z/d$ above the critical value $\sigma_c=2.86$. In **Figure 5(a)**, we can notice that, as σ augments, the values of α increase, getting a maximum at the middle of the cell. Because of the influence of external electric field, the polar angle at both borders enlarges by increasing σ highlighting the fact that even at the borders, the field is able to distort the configuration. **Figure 5 (b)** shows two interesting phenomena: (i) for $\sigma < \sigma_c$, the curves are reduced to straight lines with slope equal to $2\varphi_{0c}$, where φ_{0c} represents the azimuthal angle adopted by the MPLC at the walls of each NLC cell for values of electric field below the critical field; (ii) above the critical value, most of the molecules tend to acquire an angle $\varphi_t = -45^\circ$ for $0 < w < 0.5$ and $\varphi_t = 45^\circ$ for $0.5 < w < 1$.

Figure 6 shows the co-polarized and cross-polarized transmittances and reflectances for LCP and RCP waves impinging normally on the structure as function of the dimensionless parameter d/λ for continuous values of the electric field above the critical value σ_c (below this value, the not-shown curves are very similar to those corresponding to $\sigma=\sigma_c$). Although, the optical properties shown in **Figure 6** are qualitatively similar to those of **Figure 3** where strong anchoring conditions were considered, we notice that in the case of weak anchoring conditions, the behaviour of transmittances and reflectances in **Figure 6** is enhanced in comparison with **Figure 3**. Because of the strong influence of the electric field on the molecular orientation

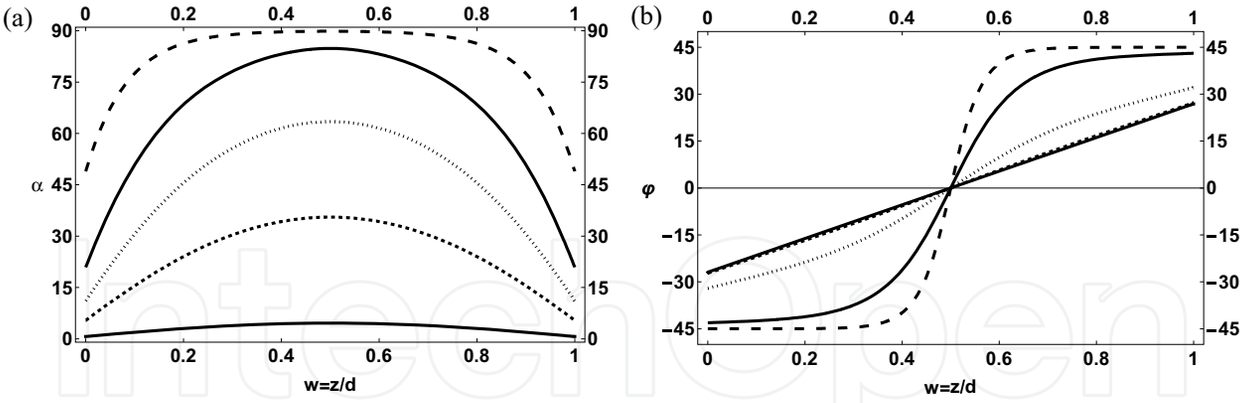

Figure 5. (a) Curves of the polar angle α as function of dimensionless variable w at different values of σ: $\sigma=\sigma_c+0.005$ (solid line), $\sigma=3.5$ (dashed line), $\sigma=4.5$ (dotted line), $\sigma=8$ (dot-dashed line) and $\sigma=13.5$ (large dashed line). (b) Curves of the azimuthal angle φ at the same values of σ as in (a).

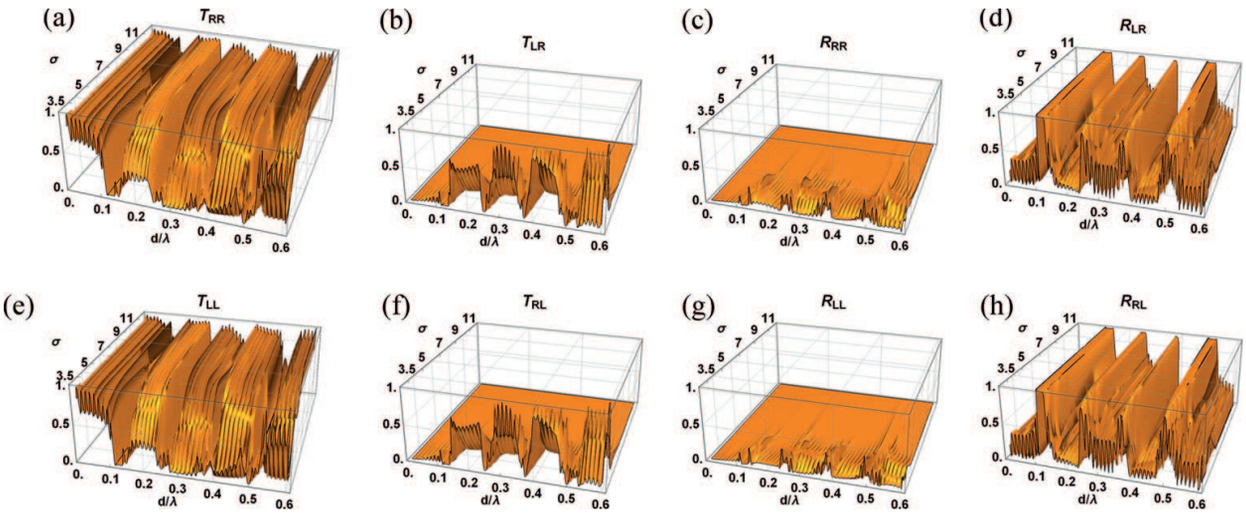

Figure 6. (a)–(h) Plots of co-polarized and cross-polarized reflectances and transmittances for LCP and RCP waves impinging normally on a MPLC as function of the dimensionless parameter d/λ and continuous values of σ within the interval $\sigma_c<\sigma<13$. Here, we consider weak anchoring conditions at the walls of each NLC.

for all values of z (including the walls of each cell), the alignment of most of the nematic molecules parallel to z-axis occurs at smaller values of electric field unlike for strong anchoring. Hence, the phenomenon of extinguishing and enhancing bands is present at smaller values of σ.

Now, we induce a defect mode in the photonic band structure by generating a defect in the MPLC in the same way as explained in Section 4.1.1. **Figure 7(a)** and **(b)** displays the defect mode induced in the photonic band of the co-polarized transmittance T_{RR} and cross-polarized reflectance R_{LR}, respectively, for LCP waves impinging normally on the MPLC. Similar to the case of strong anchoring conditions, we can observe that when the parameter σ augments the amplitude of the defect modes gets larger, and the position of the defect mode possessing the largest wavelength moves toward regions of smaller wavelengths, while the position of the other defect mode remains fixed. These facts are enhanced in comparison to those of strong anchoring assumptions because of the strong influence of the electric field on the molecular

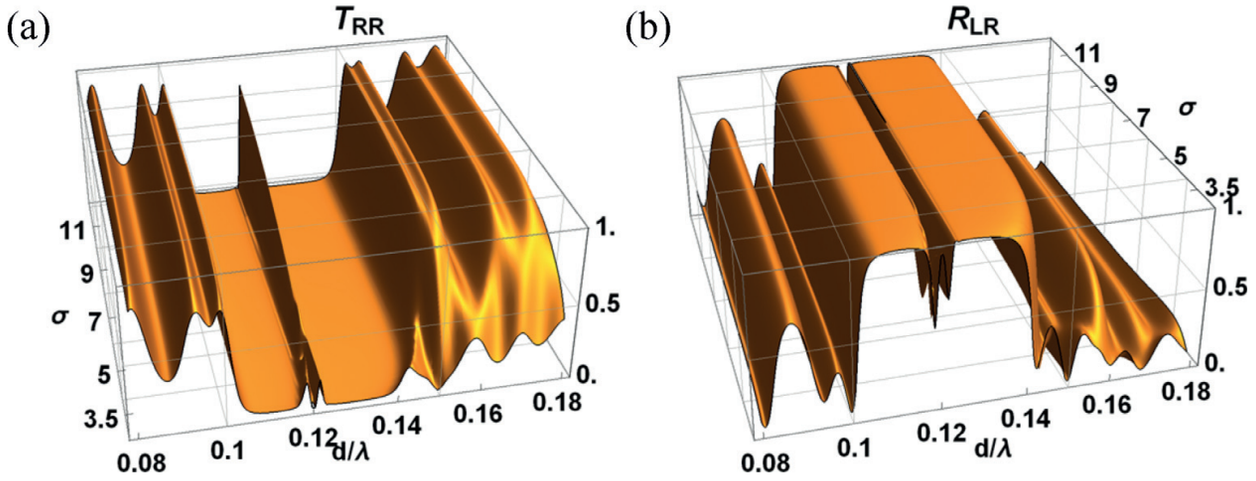

Figure 7. (a) At normal incidence, plots of co-polarized transmittance T_{RR} for LCP incident waves as function of the dimensionless parameter d/λ and continuous values of σ. (b) At normal incidence, cross-polarized reflectance R_{LR} for LCP incident waves at the same values of σ as in (a). Here, we consider weak anchoring conditions at the walls of each NLC.

orientation for all values of z, including the walls of each NLC slab in the MPLC. This implies that the defect-mode amplitude gets larger for smaller values of σ in comparison to that of the strong anchoring case.

4.2. Temperature-dependent band structure and defect mode

Here, we assume that the orientation of the director at the surfaces of each nematic cell is strongly anchored at the boundaries. In order to obtain the band structure, we apply the same mathematical procedure as depicted in Section 4.1, but in this case, we have to take into account that the director $\boldsymbol{n}$ is given by expressions (9) and (10) and the elements of dielectric tensor $\boldsymbol{\varepsilon}(z)$ depend on the wavelength and temperature [8]. By considering E7 LC mixture slabs and ZnS dielectric layers, it is found that in the interval of temperatures [15°C,50°C] and for RCP waves impinging normally, the position of the photonic bands of the co-polarized transmittance T_{RR} and cross-polarized reflectance R_{LR} (analogous to those of **Figure 3** with σ=0) can be shifted from regions of small wavelengths toward regions of higher wavelengths by increasing the thickness d of the NLC layers. In addition to this, bandwidth increases for thicker layers, and new narrower transmission bands are created in regions of smaller wavelengths. In summary, the position, the width, and the number of bands augment as the thickness d is increased. Physically, when the magnitude of d gets larger, the optical path lengths increase, and hence, the wavelength zones of destructive or constructive interference are shifted towards higher wavelength regions. For constant thickness and temperature, it is observed that as the incident angle θ augments, the photonic bands undergo a shift towards smaller wavelengths and their widths get narrower. As said previously, this behaviour results from the fact that for plane electromagnetic waves propagating obliquely with respect to the layer interfaces, only the normal component of the wave vector is involved in the photonic band formation. Thus, as the incident angle augments the relative position of the bands moves towards smaller wavelengths, and the overall band is always closed up. On the other hand, for constant thickness and a fixed incident angle, as the temperature augments, the photonic

bands move towards the short-wavelength region. Physically, since the average refractive index of the liquid crystal decreases as the temperature gets larger, the optical path length diminishes, and thus, the wavelength regions where the waves are able to undergo constructive or destructive interference shift towards smaller wavelengths zones.

In a similar way as demonstrated above, a defect mode can be induced by considering that the middle layer of the homogeneous and isotropic slabs (ZnS) has a different size compared with the remaining ones. If we consider normal incident RCP waves, for h_d=1.991h' and temperature values in the interval [15°C, 50°C], the position of the defect mode induced in the photonic band of the co-polarized transmittance T_{RR} and cross-polarized reflectance R_{LR} (analogous to those of **Figure 4** with σ=0) shifts from larger wavelengths toward smaller ones as the temperature gets increasing. Because the origin of the defect mode is the phase change due to the variation in the optical path length caused by the defective medium, the defect wavelength can be shifted towards smaller wavelength regions as the temperature is increased by taking into account that the average refractive index of the NLC decreases as temperature increases.

5. Conclusion

We presented a series of results concerning the thermal and electrical tuning of photonic band gaps and defect modes in multilayer photonic liquid crystals consisting of liquid crystal layers alternated by transparent isotropic dielectric films using nematic liquid crystal slabs in a twisted configuration. We exhibited that the position and width of the band gaps can be electrically and thermally controlled. When one of the homogeneous and isotropic slabs has a different size compared with the remaining ones, a defect mode is induced in the band structure whose wavelength can be tuned. Tuning of the transmission and reflection bands and the defect mode investigated here could be useful in the implementation of tunable optical filters and waveguides.

Author details

Carlos G. Avendaño*, Daniel Martínez and Ismael Molina

*Address all correspondence to: caravelo2000@gmail.com

Autonomous University of Mexico City, Mexico City, Mexico

References

[1] Yablonovitch E. Inhibited spontaneous emission in solid-state physics and electronics. Physical Review Letters. 1987;**58**:2059-2062. DOI: 10.1103/PhysRevLett.58.2059

[2] John S. Strong localization of photons in certain disordered dielectric superlattices. Physical Review Letters. 1987;**58**:2486-2489. DOI: 10.1103/PhysRevLett.58.2486

[3] de Gennes PG, Prost J. The Physics of Liquid Crystals. 2nd ed. Oxford: Oxford Science Publications; 1993. 597 p. ISBN: 978-0198517856

[4] Busch K, John S. Liquid-crystal photonic-band-gap materials: The tunable electromagnetic vacuum. Physical Review Letters. 1999;**83**:967-970. DOI: 10.1103/PhysRevLett.83.967

[5] Leonard SW, van Driel H, Toader O, John S, Busch K, Birner A, Gosele U. Tunable two-dimensional photonic crystals using liquid crystal infiltration. Physical Review B. 2000;**61**:R2389-R2392. DOI: 10.1103/Phys.RevB.61.R2389

[6] Ha NY, Ohtsuka Y, Jeong S, Nishimura S, Suzaki G, Takanishi Y, Ishikawa K, Takezoe H. Fabrication of a simultaneous red-green-blue reflector using single-pitched cholesteric liquid crystals. Nature Materials. 2008;**7**:43-47. DOI: 10.1038/nmat2045

[7] Molina I, Reyes JA, Avendaño CG. Electrically controlled optical bandgap in a twisted photonic liquid crystal. Journal of Applied Physics. 2011;**109**:113510-113516. DOI: 10.1063/1.3575154

[8] Avendaño C, Reyes A. Temperature-dependent optical band structure and defect mode in a one-dimensional photonic liquid crystal. Liquid Crystals. 2017;1-12. DOI: 10.1080/02678292.2017

[9] Rapini A, Papoular M. Distorsion d'une lamelle nématique sous champ magnétique conditions d'ancrage aux parois. Journal de Physique, Colloque. 1969;**30**:C4-54-C4-56. DOI: 10.1051/jphyscol:1969413

[10] Sonin AA. The Surface Physics of Liquid Crystals. Amsterdam: Gordon & Breach; 1995. ISBN: 978-2881249952

[11] Avendaño CG, Molina I, Reyes JA. Anchoring effects on the electrically controlled optical band gap in twisted photonic liquid crystals. Liquid Crystals. 2013;**40**:172-184. DOI: 10.1080/02678292.2012.735706

[12] Avendaño CG, Martinez D. Tunable omni-directional mirror based on one-dimensional photonic structure using twisted nematic liquid crystal: The anchoring effects. Applied Optics. 2014;**53**:4683-4690. DOI: 10.1364/AO.53.004683

[13] Ozaki R, Matsui T, Ozaki M, Yoshino K. Electro-tunable defect mode in one-dimensional periodic structure containing nematic liquid crystal as a defect layer. Japanese Journal of Applied Physics. 2002;**41**:L1482-L1484. DOI: 10.1143/JJAP.41.L1482

[14] Arkhipkin VG, Gunyakov VA, Myslivets SA, Gerasimov VP, Zyryanov VY, Vetrov SY, Shabanov VF. One-dimensional photonic crystals with a planar oriented nematic layer: Temperature and angular dependence of the spectra of defect modes. JETP. 2008;**106**:388-398. DOI: 10.1134/S1063776108020179

[15] Lin Y-T, Chang W-Y, Wu C-Y, Zyryanov VY, Lee W. Optical properties of one-dimensional photonic crystal with a twisted-nematic defect layer. Optics Express. 2010;**18**:26959-26964. DOI: 10.1364/OE.18.026959

[16] Timofeev IV, Lin Y-T, Gunyakov VA, Myslivets SA, Arkhipkin VG, Vetrov SY, Lee W, Zyryanov VY. Voltage-induce defect mode coupling in a one-dimensional photonic crystal with a twisted-nematic defect layer. Physical Review E. 2012;**85**:011705. DOI: 10.1103/PhysRevE.85.011705

[17] Stewart IW. The Static and Dynamic Continuum Theory of Liquid Crystals: A Mathematical Introduction. 1st ed. New York: Taylor & Francis Group; 2004. 351 p. ISBN: 978-0748408962

[18] Rasing T, Muševič I. Surfaces and Interfaces of Liquid Crystals. 1st ed. New York: Springer; 2004. p. 298. DOI: 10.1007/978-3-662-10157-5

[19] Castellano JA. Surface anchoring of liquid crystal molecules on various substrates. Molecular Crystals and Liquid Crystals. 1983;**94**:33-41. DOI: 10.1080/00268948308084245

[20] Takatoh K, Hasegawa M, Koden M, Itoh N, Hasegawa R, Sakamoto M. Alignment Technologies and Applications of Liquid Crystals Devices. 1st ed. New York: Taylor & Francis Inc.; 2005. p. 320. DOI: 10.1201/9781420023015

[21] Rüetschi M, Grütter P, Fünfschilling J, Güntherodt H. Creation of liquid crystal waveguides with scanning force microscopy. Science. 1994;**265**:512-514. DOI: 10.1126/science.265.5171.512

[22] Pidduck AJ, Haslam SD, Bryan-Brown GP, Bannister R, Kitely ID. Control of liquid crystal alignment by polyimide surface modification using atomic force microscopy. Applied Physics Letters. 1997;**71**:2907. DOI: 10.1063/1.120212

[23] Gibbons WM, Shannon PJ, Sun S, Swtlin BJ. Surface-mediated alignment of nematic liquid crystals with polarized laser light. Nature. 1991;**351**:49-50. DOI: 10.1038/351049a0

[24] Chigrinov VG, Kozenkov VM, Kwok H-S. Photoalignement of Liquid Crystalline Materials: Physics and Applications. West Sussex: John Wiley & Sons; 2008. p. 248. DOI: 10.1002/9780470751800

[25] Vilfan M, Mertelj A, Copic M. Dynamic light scattering measurements of azimuthal and zenithal anchoring of nematic liquid crystals. Physical Review E. 2002;**65**:041712-1-041712-7. DOI: 10.1103/PhysRevE.65.041712

[26] Zhao W, Wu C, Iwamoto M. Weak boundary anchoring, twisted nematic effect and homeotropic to twisted-planar transition. Physical Review E. 2002;**65**:031709. DOI: 10.1103/PhysRevE.65.031709

[27] Baek S-I, Kim S-J, Kim J-H. Measurement of anchoring coefficient of homeotropically aligned nematic liquid crystal using a polarizing optical microscope in reflective mode. AIP Advances. 2015;**5**:097170. DOI: 10.1063/1.4931950

[28] Chuang SL. Physics of Photonic Devices. 2nd ed. New Jersey: John Wiley & Sons; 2009. p. 840

[29] Hecht E, Zajac A. Óptica. 3rd ed. Madrid: Addison Wesley Iberoamericana; 2010. 722 p. ISBN: 84-7829-025-7

[30] Marcuvitz N, Schwinger J. On the representation of electric and magnetic field produced by currents and discontinuities in waveguides. Journal of Applied Physics. 1951;**22**:806-819. DOI: 10.1063/1.1700052

[31] Altman C, Suchy K. Reciprocity, Spatial Mapping and Time Reversal in Electromagnetics. 2nd ed. Heidelberg: Springer; 2011. DOI: 10.1007/978-94-007-1530-1

[32] Berreman DW, Scheffer TJ. Bragg reflection of light from single-domain cholesteric liquid-crystal films. Physical Reviews Letters. 1970;**25**:577-581. DOI: 10.1103/PhysRevLett. 25.902.4

[33] Avendaño CG, Ponti S, Reyes JA, Oldano C. Multiplet structure of the defect modes in 1D helical photonic crystals with twist defects. Journal of Physics A: Mathematical and General. 2005;**38**:8821-8840. DOI: 10.1088/0305-4470/38/41/001

[34] Nastishin YA, Polak RD, Shiyanovskii SV, Bodnar VH, Lavrentovich OD. Nematic polar anchoring strength measured by electric field techniques. Journal of Applied Physics. 1999;**86**:4199-4213. DOI: 10.1063/1.371347

IntechOpen